6-1-2010

Modeling radiation belt radial diffusion in ULF wave fields: 2. Estimating rates of radial diffusion using combined MHD and particle codes

Chia-Lin L. Huang
hcl@guero.sr.unh.edu

Harlan E. Spence
University of New Hampshire, harlan.spence@unh.edu

Mary K. Hudson

Scot R. Elkington

Recommended Citation
Huang, C.-L., H. E. Spence, M. K. Hudson, and S. R. Elkington (2010), Modeling radiation belt radial diffusion in ULF wave fields: 2. Estimating rates of radial diffusion using combined MHD and particle codes, J. Geophys. Res., 115, A06216, doi:10.1029/2009JA014918.

JOURNAL OF GEOPHYSICAL RESEARCH, VOL. 115, A06216, doi:10.1029/2009JA014918, 2010

Modeling radiation belt radial diffusion in ULF wave fields: 2. Estimating rates of radial diffusion using combined MHD and particle codes

Chia-Lin Huang,[1] Harlan E. Spence,[1,2] Mary K. Hudson,[3] and Scot R. Elkington[4]

Received 21 September 2009; revised 6 May 2010; accepted 12 May 2010; published 25 June 2010.

[1] Quantifying radial transport of radiation belt electrons in ULF wave fields is essential for understanding the variability of the trapped relativistic electrons. To estimate the radial diffusion coefficients (D_{LL}), we follow MeV electrons in realistic magnetospheric configurations and wave fields calculated from a global MHD code. We create idealized pressure-driven MHD simulations for controlled solar wind velocities (hereafter referred to as pressure-driven V_x simulations) with ULF waves that are comparable to GOES data under similar conditions, by driving the MHD code with synthetic pressure profiles that mimic the pressure variations of a particular solar wind velocity. The ULF wave amplitude, in both magnetic and electric fields, increases at larger radial distance and during intervals with higher solar wind velocity and pressure fluctuations. To calculate D_{LL} as a function of solar wind velocity (V_x = 400 and 600 km/s), we follow 90 degree pitch angle electrons in magnetic and electric fields of the pressure-driven V_x simulations. D_{LL} is higher at larger radial distance and for the case with higher solar wind velocity and pressure variations. Our simulated D_{LL} values are relatively small compared to previous studies which used larger wave fields in their estimations. For comparison, we scale our D_{LL} values to match the wave amplitudes of the previous studies with those of the idealized MHD simulations. After the scaling, our D_{LL} values for V_x = 600 km/s are comparable to the D_{LL} values derived from Polar measurements during nonstorm intervals. This demonstrates the use of MHD models to quantify the effect of pressure-driven ULF waves on radiation belt electrons and thus to differentiate the radial diffusive process from other mechanisms.

Citation: Huang, C.-L., H. E. Spence, M. K. Hudson, and S. R. Elkington (2010), Modeling radiation belt radial diffusion in ULF wave fields: 2. Estimating rates of radial diffusion using combined MHD and particle codes, *J. Geophys. Res.*, *115*, A06216, doi:10.1029/2009JA014918.

1. Introduction

[2] Identifying and determining the acceleration, transport and loss mechanisms that populate, maintain, and modify the radiation belt electrons remains a major open scientific question. Fluctuations in magnetospheric electric and magnetic fields can lead to substantial reconfiguration of the outer electron belt. Wave-particle interactions with periods comparable to the particle gyration time play an important role in the overall dynamics of the radiation belts [*Horne and Thorne*, 1998; *Summers et al.*, 1998]. Magnetospheric waves in the ULF (mHz) frequency range can also provide a reservoir of energy capable of accelerating particles on time scales of a few hours to several days [*Baker et al.*, 1998; *Rostoker et al.*, 1998]. Reviews on acceleration and loss of radiation belt electrons are available which provide extensive background on the subject [e.g., *Friedel et al.*, 2002; *Hudson et al.*, 2008; *Shprits et al.*, 2008a, 2008b].

[3] Using particle tracing codes, a number of hypotheses have been proposed to explain the physical connection between ULF waves and relativistic electrons. For example, *Hudson et al.* [1999, 2000] modeled the evolution of relativistic electron fluxes in the equatorial plane using the results of MHD simulations as field input. They proposed a drift-resonant acceleration mechanism resulting from ULF waves in the MHD simulations and the radial asymmetries in the electric field. *Elkington et al.* [1999, 2003] found the asymmetric resonances with toroidal and poloidal modes can lead to sufficient radial diffusion that may be appropriate to explain the observed electron fluxes during geomagnetic storms. Quantifying the effect of ULF waves on the outer electron belt is essential for differentiating such mechanism

[1]Center for Space Physics, Boston University, Boston, Massachusetts, USA.
[2]Also at Institute for the Study of Earth, Oceans, and Space, University of New Hampshire, Durham, New Hampshire.
[3]Department of Physics and Astronomy, Dartmouth College, Hanover, New Hampshire, USA.
[4]Laboratory for Atmospheric and Space Physics, University of Colorado, Boulder, Colorado, USA.

0148-0227/10/2009JA014918

from others, thus understanding variability of the trapped relativistic electrons.

[4] The physical link between wave activity and charged particle dynamics is illuminated via diffusion theory. Diffusion theory is a treatment of the time evolution of a distribution of particles whose trajectories are disturbed by innumerable small, random changes [*Walt*, 1994]. The pioneering work on diffusive transport of the radiation belts [*Kellogg*, 1959; *Parker*, 1960] revealed the importance of wave-particle interactions in influencing the dynamics of the relativistic electrons. Through electric and magnetic field perturbations in the frequency range of ULF waves, a particle's third adiabatic invariant may be violated while its first two invariants are conserved. During such a process, electrons gain or lose energy as they diffuse inward or outward across drift shells in radial distance [*Fälthammar*, 1965; *Nakada and Mead*, 1965]. Radial diffusion with conservation of the first two adiabatic invariants [see *Schulz and Lanzerotti*, 1974] is described with the following equations:

$$\frac{\partial f}{\partial t} = L^{*2}\frac{\partial}{\partial L^*}\left[D_{LL}L^{*-2}\frac{\partial f}{\partial L^*}\right] \tag{1}$$

$$D_{LL} = \frac{\left\langle \left(L^* - L_0^*\right)^2 \right\rangle}{2\tau} \qquad \left[day^{-1}\right]. \tag{2}$$

Equation (1) is the radial diffusion equation of f and equation (2) is the expression for the radial diffusion coefficient. The phase space density, f, is a function of the three adiabatic invariants which exclude the adiabatic effect due to the field configuration. The diffusion rate of phase space density is determined by the radial diffusion coefficient D_{LL}. L_0^* and L^* are the initial and final radial positions before and after a given amount of time, τ.

[5] Estimates of the radial diffusion coefficient of radiation belt electrons due to magnetic and electric fluctuations (D_{LL}^M and D_{LL}^E) have been performed using both theoretical derivations and particle observations over the past several decades. A complete theoretical treatment of the calculation of D_{LL}^M and D_{LL}^E is outlined by *Schulz and Lanzerotti* [1974]. Based on observational evidence, there also have been substantial attempts to determine particle diffusion rates using a number of different techniques. The radial diffusion rate increases with L, with an L dependence ranging between L^6 and L^{11}. The large deviations between these studies indicate that the experimental uncertainties are large and the observed diffusion coefficient is time dependent. There are many approximations and assumptions used in deriving theoretical values of D_{LL}, so it is not surprising that theoretical and experimental results are so different. For more extensive discussion of this subject, papers by *Lanzerotti et al.* [1970], *Brautigam and Albert* [2000], *Elkington et al.* [2003], and *Perry et al.* [2005] along with the reference therein provide a comprehensive review.

[6] The cause of the different estimates of diffusion rate might be the use of the three fundamental elements needed to obtain D_{LL} values empirically: magnetic field model, wave field model, and calculation method of solving D_{LL}. First, a magnetic field model is needed to follow a test particle's global trajectory or to connect electron measurements from different regions of the magnetosphere to the equatorial plane. An accurate magnetospheric model is important to correctly calculate the adiabatic invariants, which will greatly affect the estimation of phase space density. The magnetic field models range from a simple dipole field, to advanced empirical models, to more sophisticated global MHD codes which can produce a range of dramatically different field configurations. The second requirement is a wave field model which is needed to characterize the wave spectrum and power in three-dimensional space during levels of magnetospheric activity. An accurate description of the small and random perturbations in electric or magnetic field as a function of time and space is the key element in quantifying a particle's diffusive process. However, such comprehensive global maps of wave power are not available due to the limitations inherent in single-point measurements. Finally, calculation of the radial diffusion coefficient can be accomplished by using either equation (1) or (2). The first way to derive D_{LL} is to solve equation (1) using observed phase space density f as functions of time and radial distance. However, converting particle measurements to phase space density is not an easy task due to the inaccuracies of field models [*Green and Kivelson*, 2004]. The other method is to follow test particles in given electric and magnetic fields and calculate D_{LL} using equation (2). As a result, when using calculated radial diffusion coefficients to study radial transport, all above factors that are used in the calculation should be considered. Later in the paper, a detailed comparison of recent studies and these three elements will be discussed.

[7] Quantitative statistical studies show that the Lyon-Fedder-Mobbary (LFM) MHD code makes reasonable predictions of the magnetic fields and ULF wave fields at geosynchronous orbit during nonstorm intervals [*Huang et al.*, 2006, 2010]. Such studies are encouraging for the radiation belt community, because being able to predict reasonable field configuration and ULF wave power is an important element in understanding the role of ULF waves on the radial transport of outer belt electrons. Based on the previous studies, we use the MHD magnetic and electric fields as the inputs to a test particle tracing code to simulate the effects of ULF waves on radiation belt electrons in a realistic fashion. We generate idealized pressure-driven MHD simulations for particular solar wind velocities (hereafter referred to as pressure-driven V_x simulations) with ULF waves that are comparable to GOES data under similar conditions. Then we follow the test particles in the MHD fields to determine the radial diffusion rate as a function of solar wind velocity, $D_{LL}(V_x)$. Finally, we compare the D_{LL} values calculated from the combined MHD and particle codes with previous estimations under similar conditions to quantify radial diffusion of relativistic electrons in ULF wave fields.

2. MHD Pressure-Driven V_x Simulations

[8] The Lyon-Fedder-Mobbary (LFM) code [*Lyon et al.*, 2004] is a three-dimensional magnetohydrodynamic (MHD) code that simulates Earth's magnetosphere and provides global, time-dependent, and self-consistent electric and magnetic fields that are needed for this study. From the work of *Huang et al.* [2006], the capabilities of the LFM

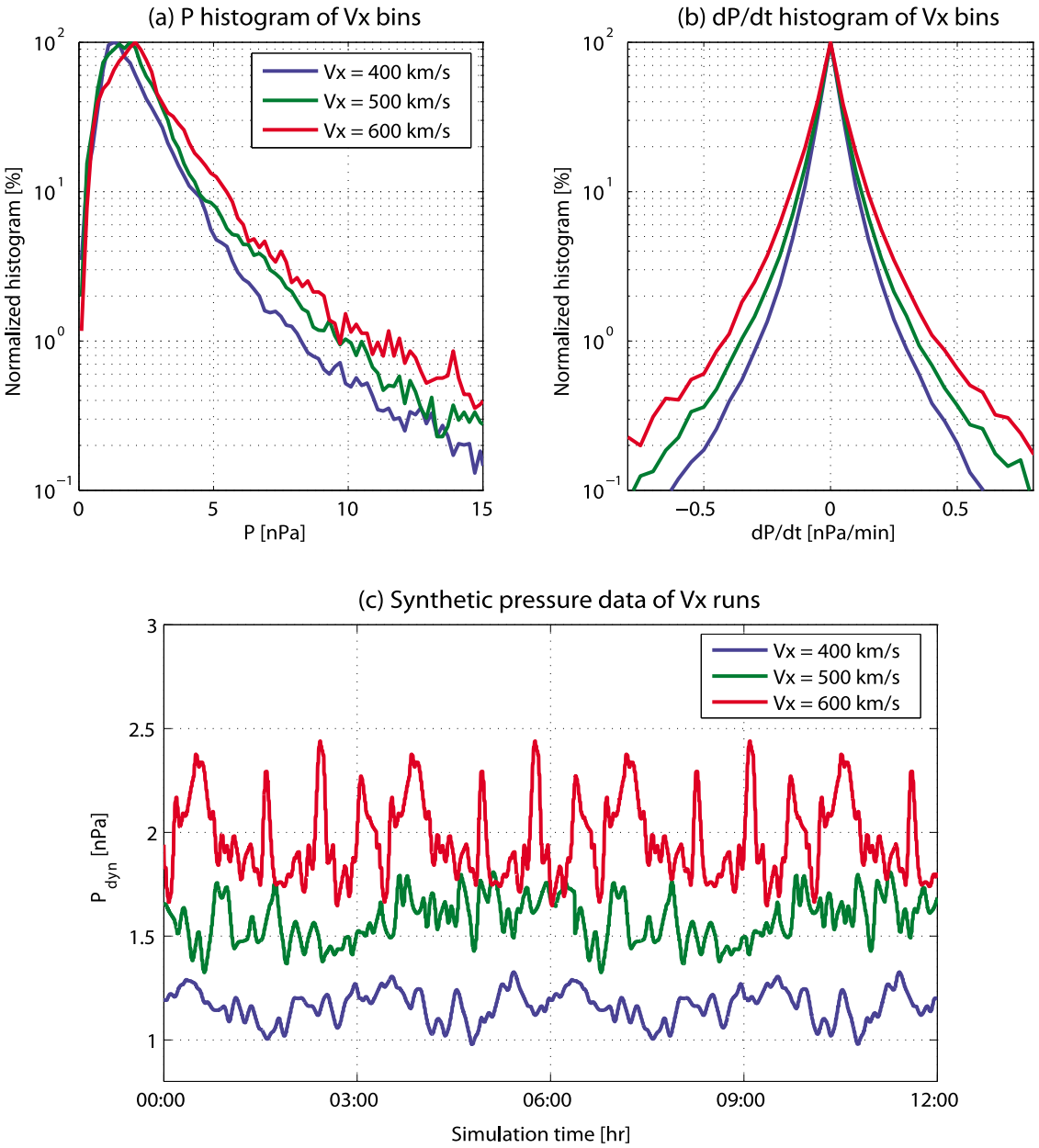

Figure 1. (a) and (b) Solar wind dynamic pressure distributions as a function of solar wind velocity (V_x = 400, 500 and 600 km/s in blue, green and red, respectively) based on 9 years of Wind data. Figure 1a shows the dynamic pressure (P_d) distributions normalized by the maximum value of the histogram. Figure 1b shows the normalized distributions of change of pressure with time (dP_d/dt) includes both positive and negative values. The synthetic solar wind pressure data generated based on the Wind data are plotted in Figure 1c.

MHD code to predict the ambient magnetic field were examined by statistical comparisons with GOES data. Quantitative statistical studies of the MHD simulations show that MHD field lines are consistently under stretched, especially during storm time on the nightside, a likely consequence of an insufficient representation of the inner magnetospheric current systems. However, the LFM code makes reasonable predictions of magnetic fields at geosynchronous orbit during nonstorm time intervals. For the wave field predictions, *Huang et al.* [2010] quantified ULF wave power (f = 0.5–8.3 mHz) in GOES observations and LFM magnetic fields for a 27 day nonstorm interval. The LFM code does well at reproducing, in a statistical sense, the ULF wave power observed by GOES. This study suggests the LFM code is capable of modeling variability in the magnetosphere on ULF wave time scale during typical solar wind conditions. Based on the findings of *Huang et al.* [2006, 2010], we use the MHD wave fields during nonstorm time to study ULF wave effects on radiation belt electrons.

[9] *Paulikas and Blake* [1979] demonstrated that the relativistic electron flux enhancements are highly correlated with

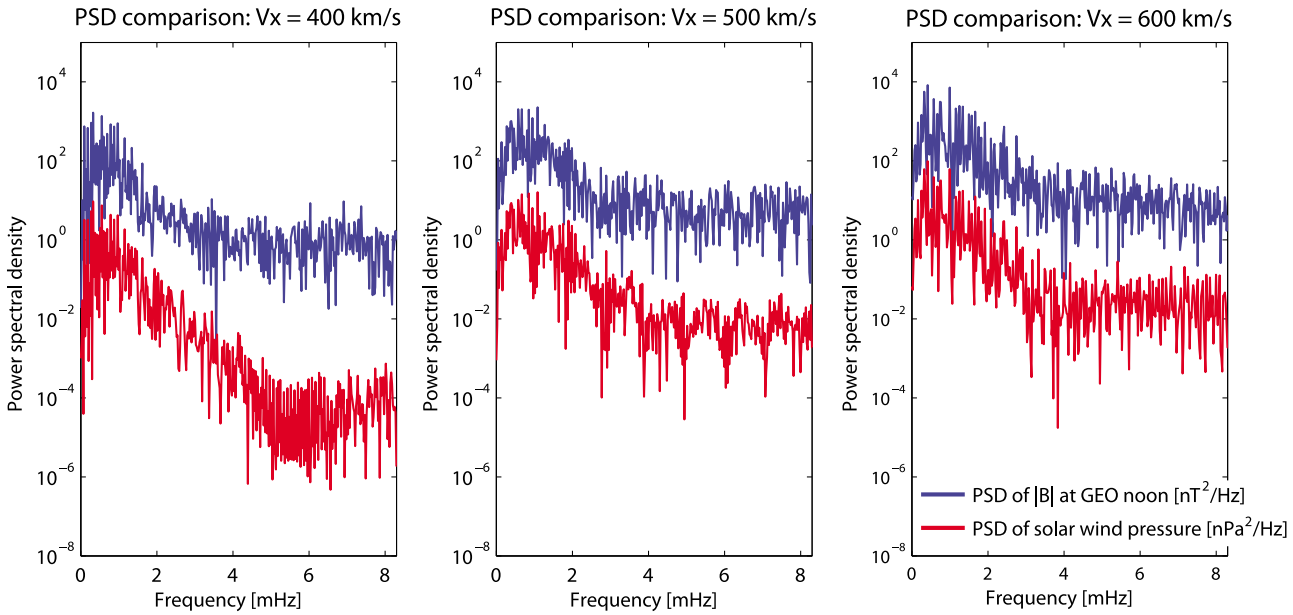

Figure 2. Comparisons of power spectral density from synthetic solar wind pressure data (red) and ULF wave at local noon of geosynchronous orbit predicted by the MHD simulations (blue). The PSDs are plotted on the same scale with different units, nT^2/Hz and nPa^2/Hz for solar wind pressure and ULF wave at GEO noon, respectively.

solar wind velocity. Based on a statistical study of GOES magnetic field data, *Huang et al.* [2010] showed that solar wind velocity is indeed one of the best sorting parameters of ULF wave power. Therefore, we choose solar wind velocity as an ordering parameter to create idealized MHD simulations and to estimate the radial diffusion rate of radiation belt electrons. In this work, we create ULF wave activity as a function of solar wind velocity by driving the MHD code with synthetic solar wind dynamic pressure based on statistical velocity distributions observed by the Wind satellite. To isolate dynamic pressure from other factors which might generate waves, the IMF B_z is held northward throughout the simulations. After creating the idealized pressure-driven V_x simulations, we examine the wave predictions with GOES statistical data under similar conditions to test the model validity.

2.1. Synthetic Solar Wind Pressure Variations

[10] To compare directly the measured radial diffusion rates of radiation belt electrons with those inferred from models, we would need a long-period simulation (much longer than a particle's drift period) that possesses similar solar wind conditions throughout the event. This type of solar wind input is hard to find in reality from satellite measurements, for example, 12 h long solar wind data of steady solar wind velocities at 600 km/s. An alternative is to run the LFM code with synthetic solar wind inputs based on observations. In particular, we drive MHD simulations with idealized inputs based on statistical solar wind data that represent key statistical aspects of the solar wind characteristics during particular conditions. Then, we can use the realistic MHD simulations to quantify the radial transport of radiation belt electrons during different solar wind conditions or geomagnetic activity levels. In this study, we concentrate on the solar wind dynamic pressure variations as a function of solar wind velocity.

[11] To build the statistical distribution of solar wind dynamic pressure, we use 9 years (1995–2003) of Wind data, at 2 min time resolution. A few selection criteria are applied: Wind satellite in the upstream solar wind (≥20 R_E), and, IMF $B_z > 0$ nT. To better understand and construct the variations in dynamic pressure, we explore the pressure magnitudes and the scales of pressure fluctuations for different solar wind velocities. Figure 1a and 1b show the histograms of pressure magnitude (P_d) and pressure change with time (dP_d/dt), respectively, for three V_x bins (400, 500, 600 km/s with bin size ±50 km/s). The histograms are normalized by the maximum bin value in each histogram. Both pressure value and fluctuation distributions show monotonic enhancement with the increase of solar wind velocity. During high velocity intervals, the pressure values are higher and the pressure variations are stronger and sharper.

[12] Based on these pressure distributions, we build synthetic pressure variations as a function of solar wind velocity. Time series of pressure variations are the combination of many pressure changes (ΔP_d) as the products of pressure change with time and durations ($\Delta P_d = \pm \frac{dP_d}{dt} \times dt$). To obtain series of ΔP_d values, we randomly pick dP_d/dt values from Figure 1b according to the occurrence rate, and times durations (dt) between 1 to 5 minutes. We then build an idealized pressure time series by connecting ΔP_d values together consecutively, starting and ending with the most probable pressure for each V_x bin, e.g., 1.3 nPa for V_x = 400 km/s. To keep the pressure data within physically reasonable values, we set an upper and a lower pressure limit. These limits are the 50% level of each V_x pressure histogram in Figure 1a, e.g., $P_{d,up}$ and $P_{d,low}$ are 0.9 and 1.6 nPa for V_x =

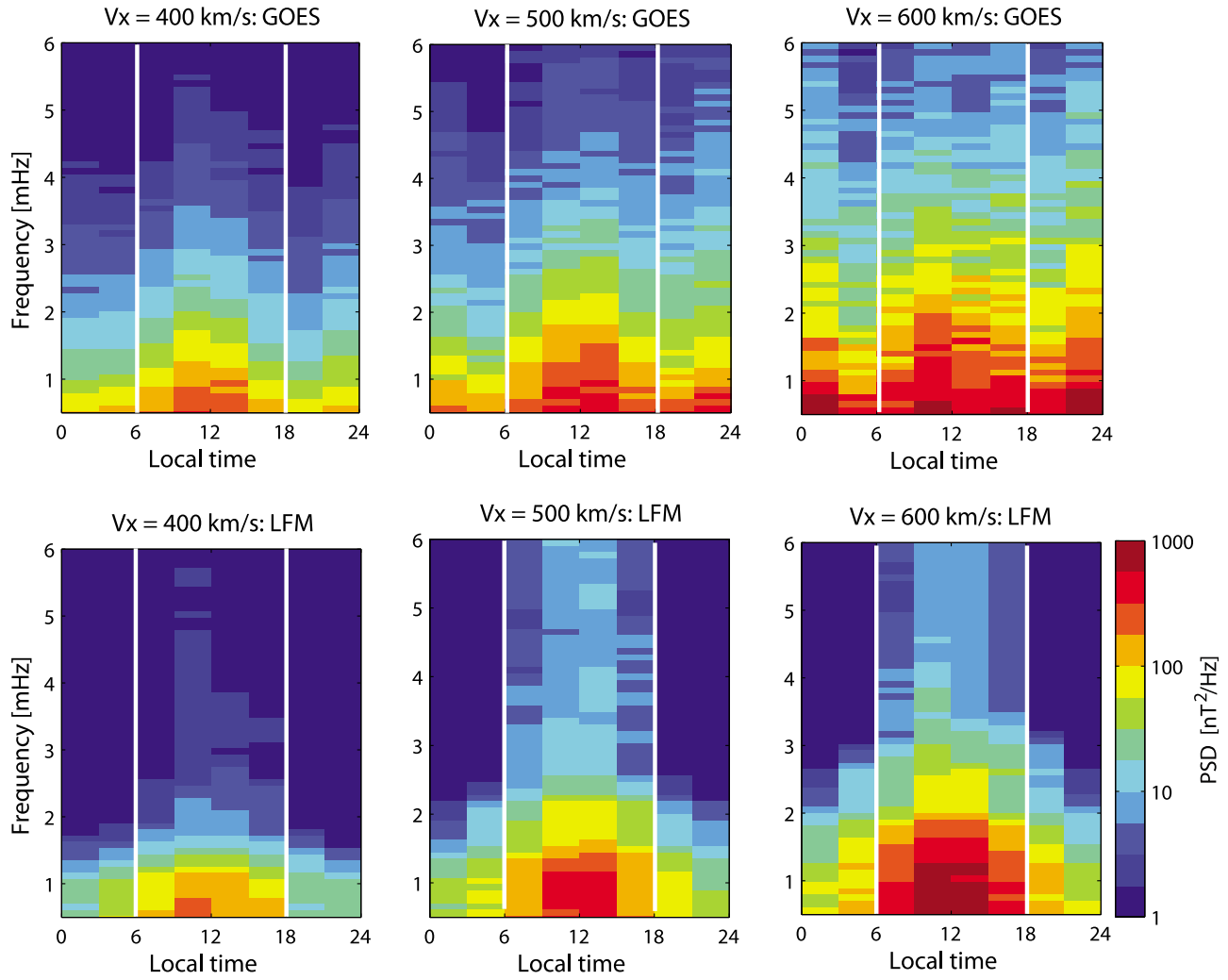

Figure 3. (top) Power spectral density comparisons of GOES statistical results and (bottom) the idealized pressure-driven V_x MHD simulations for solar wind velocities of (left) 400, (middle) 500, and (right) 600 km/s. Wave power as a function of local time and frequency is shown on a colored logarithmic scale from 10^0 to 10^3 nT^2/Hz. The white vertical lines separate the dayside and nightside magnetosphere.

400 km/s. Finally, we do a 3-point running average to ensure smoothness of the idealized data time series. Figure 1c shows the ~12 hour synthetic solar wind pressure data for different solar wind velocities. Similar to the statistical distributions from the Wind observations, the dynamic pressure values and fluctuations are higher for higher velocity intervals, and vice versa. In addition, the pressure fluctuation (dP_d/dt) distributions between the synthetic data and statistical average of 9 year Wind observations are comparable for all three velocity bins.

[13] The synthetic pressure data are the only time-varying parameter that drives the MHD simulations. For each idealized V_x simulations, we calculate the number densities from dynamic pressure variations in Figure 1c by assuming strictly constant solar wind velocity for each V_x run (i.e., 400, 500, and 600 km/s). For the other model input parameters, solar wind V_y and V_z, IMF B_x and B_y are zero; and B_z is +2 nT throughout the interval to isolate the pressure-driven wave. We then drive the MHD code with the inputs to generate three ~12 hour long simulations as a function of solar wind velocity.

[14] To analyze the pressure-driven ULF waves generated in the MHD simulations, we compare the wave spectrum of the upstream solar wind pressure and magnetic field in the modeled magnetosphere. After running a high pass filter to attenuate frequencies lower than some desired cutoff frequency (0.5 mHz is the lower limit of ULF waves considered in this study), we perform a Fast Fourier Transform to obtain the power spectral density (PSD). PSDs of the synthetic solar wind pressure data and the dayside magnetic field predicted by the MHD simulations are plotted in Figure 2 as a function of solar wind velocity (V_x = 400, 500, and 600 km/s, from left to right). We pick magnetic field at local noon of geosynchronous orbit (6.6, 0, 0)R_E to represent the ULF wave power because the dayside magnetosphere is most directly driven by solar wind pressure and because geosynchronous orbit is inside the outer electron belt. The wave power in solar wind pressure is higher at all frequencies

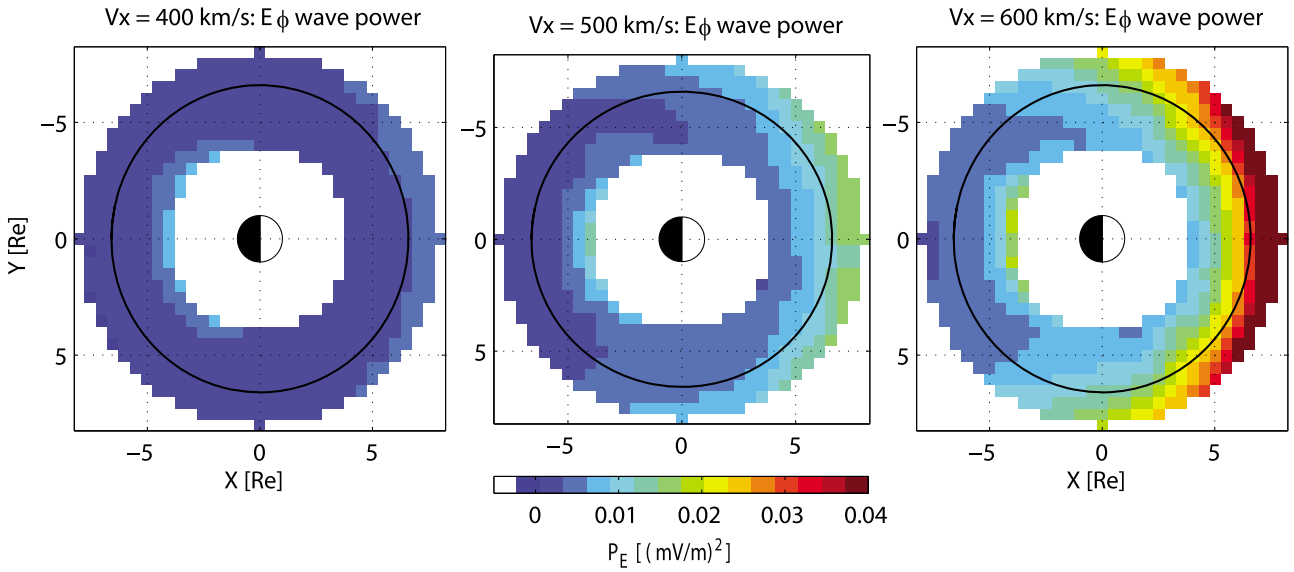

Figure 4. Spatial distributions of ULF wave power integrated over frequency range of 0.5 and 8.3 mHz in the E_ϕ component for the idealized pressure-driven V_x MHD simulations. The integrated wave power are plotted in the magnetic equatorial plane. The black circle has radius of 6.6 R_E which locates geosynchronous orbit. The color scales are the same for all panels, from 0 to 0.04 $(mV/m)^2$.

for higher solar wind V_x simulations. As a direct response, the ULF wave power in the dayside magnetosphere also increases with the enhancement of solar wind velocity and pressure wave power.

[15] Similar to the results of *Elkington et al.* [1999] and *Kepko et al.* [2002], the PSD fluctuations of the synthetic solar wind pressure and dayside magnetic field are highly correlated, especially for the MHD simulations of V_x = 500 and 600 km/s. In the V_x = 400 km/s simulation, wave power in the solar wind pressure in weak at frequencies higher than 4 mHz while the ULF wave power remains nearly constant. Instabilities in the MHD modeled magnetosphere may generate ULF wave power at the higher frequencies in this simulation to account for the nonsolar wind driven ULF wave power. Detailed investigation is needed in the future to fully understand the response of the global MHD code to solar wind pressure variations in this higher frequency range. Nevertheless, the V_x MHD simulations show that pressure-driven ULF wave power is closely correlated with the synthetic solar wind pressure wave power.

2.2. Comparisons of GOES Data and MHD Model Predictions

[16] To examine the ULF wave predictions of the pressure-driven V_x simulations, we compare the ULF wave powers between model results at geosynchronous orbit and GOES data. The MHD simulations have constant solar wind velocity inputs as V_x = 400, 500, and 600 km/s and IMF *Bz* inputs as +2 nT. To compare the data/model under similar conditions, we sorted 9 years (1995–2003) of magnetic field data from GOES-8, 9, and 10 satellites under northward IMF B_z by the same solar wind velocity bins (400, 500, 600 km/s with bin size ±50 km/s). Following the wave analysis method from *Huang et al.* [2010], we (1) sort the data according to their local times and divide data into 3 h intervals; (2) exclude intervals that have a sudden or discontinuous change in the time series data; (3) detrend the data with a 3rd degree polynomial fit to eliminate slow variations cause by the diurnal variation of the magnetic field at geosynchronous orbit; (4) despike data points which exceed three standard deviations; (5) run a high pass filter at 0.5 mHz; and (6) perform a Fast Fourier Transform to obtain the power spectral density in units of nT^2/Hz. Figure 3 illustrates the power spectral densities of field magnitudes of GOES statistical results (Figure 3 (top)) and the LFM predictions at geosynchronous orbit (Figure 3 (bottom)).

[17] Although ULF waves are a second-order quantity produced by the LFM code, we may reasonably expect the model's wave statistical properties to agree with observations [*Huang et al.*, 2010]. Figure 3 shows that the modeled and observed ULF wave power on the dayside magnetosphere are comparable under similar conditions. The nightside wave power does not agree very well because we are comparing the "mostly" IMF northward data with the "purely" IMF northward simulation results. Even when the average IMF B_z of a 3 hour interval is positive, it can still contain significant subintervals of negative B_z values. On the other hand, the simulations are driven by purely positive IMF B_z by deliberate design to produce solely pressure-driven waves. In this model limit, the pressure variations should excite waves principally in the dayside magnetosphere (i.e., where geostationary orbit is closest to the magnetopause). In the work of *Huang et al.* [2010], when simulating a 27 day real event which includes southward IMF B_z, the LFM code did create reasonable wave activity in the nightside magnetosphere when compared to GOES data. Therefore, for these ideal northward IMF simulations, it is appropriate to compare the model results with GOES statistical data in the dayside magnetosphere (0600–1800 LT) only. The LFM code predicts ULF waves at geosynchronous orbit reasonably well, so we assume the MHD fields are realistic at the outer radiation belt simulation

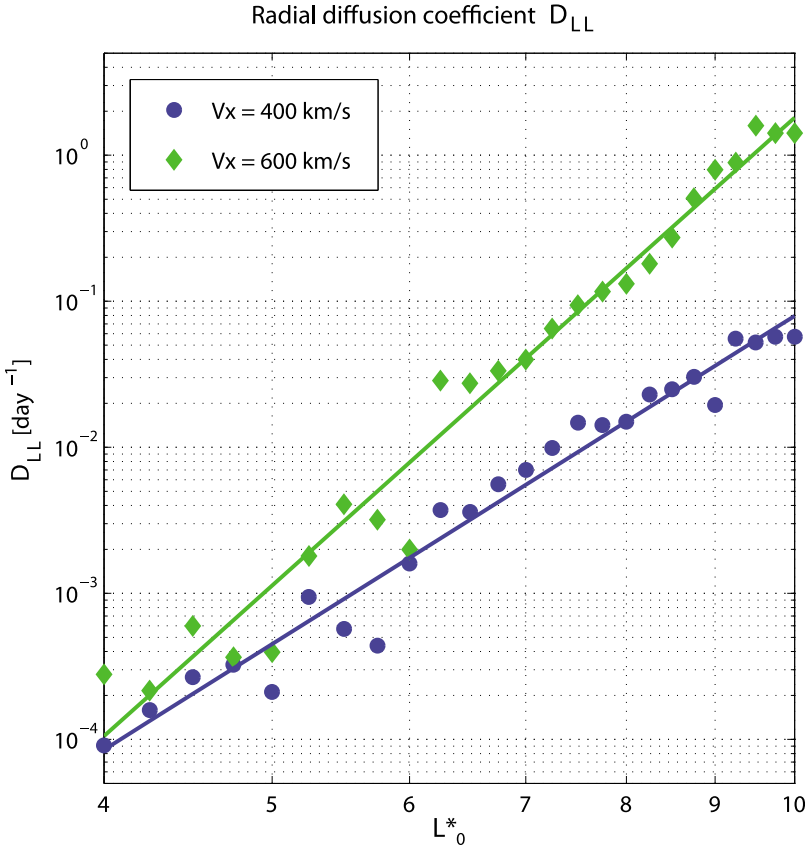

Figure 5. Radial diffusion coefficients (D_{LL}) calculated from following electrons in the fields of the pressure-driven V_x simulations. Blue circles and green diamonds are the D_{LL} values of the V_x = 400 and 600 km/s runs, respectively. The lines are the least squares fit of the D_{LL} values in a logarithmic scale.

domain (L = 4–8). This assumption may not be physically accurate at the lower L because the LFM code we used does not include a plasmasphere model. In addition to the comparisons at geosynchronous orbit, we also explore the extended spatial distribution and integrated ULF wave power of these pressure-driven V_x simulations in electric field.

2.3. Spatial Distribution of ULF Waves in E_ϕ

[18] Electrons executing azimuthal gradient and curvature drift in the radiation belt will undergo the greatest acceleration when the electric field points in the direction of the electron drift path. Therefore, electric fields in the azimuthal direction are believed to have the largest effect on radiation belt electrons [*Elkington et al.*, 2003]. For that reason, we explore the spatial distribution of ULF wave power in E_ϕ in the equatorial plane which has the largest effect on 90 degree pitch angle electrons. Figure 4 shows the integrated ULF wave power of the pressure-driven V_x simulations in the E_ϕ component in the magnetic equatorial plane.

[19] Overall, the MHD simulations with higher solar wind velocity have higher integrated ULF wave power, especially on the dayside magnetosphere. In these northward IMF simulations, solar wind dynamic pressure drives the variations in magnetic field configuration and generates inductive electric fields in the magnetosphere. The electric field perturbations are stronger near the magnetopause and weaker in the near Earth region as the energy decreases when getting further away from the source. In contrast, when IMF B_z is negative, the E_ϕ wave power in the nightside magnetosphere should vary with the magnitude and duration of southward IMF B_z as a result of other internal magnetospheric wave sources. These E_ϕ wave power maps indicate the level of wave field that energetic particles will experience and the amount of particle radial transport to expect, when following the test particles in the field results of the pressure-driven V_x simulations. To quantify the effects of ULF waves on radiation belt electrons, we pick the MHD V_x = 400 and 600 simulations representing realistic values of typical and higher solar wind speed to calculate the particle transport in such events.

3. Quantify Radial Transport Using Combined MHD and Particle Codes

[20] To quantify electron radial transport in ULF wave fields, we use a two-dimensional guiding center particle tracing code [*Elkington et al.*, 2004]. The fully relativistic particle tracing code solves a charged particle's equation of motion using a fourth-order Runge-Kutta integrator. We use the magnetic and electric field predictions of the MHD simulations to follow trajectories of 90 degree pitch angle electrons. *Perry et al.* [2006] numerically quantified the pitch angle dependence of the radial diffusion coefficient by following electron guiding center motion in a background dipole magnetic field, incorporating frequency and L-dependent ULF wave. Similar to *Schulz and Lanzerotti* [1974], the

Table 1. Summary of Recent Estimations on Radial Diffusion Coefficients in Distinguish Properties[a]

Reference	Magnetic field model	Wave field	Calculation	*L*-shell	*M* [MeV/G]	*dB* or *dE* at GEO	D_{LL} [day^{-1}]	*L*-dependence
Selesnick et al. [1997]	T89 (Kp = 2)	3 month real event	Diffusion equation	3–6.5	6000	Nonstorm, *dB* ~10 nT	10^{-4} to 10^{-0}	$L^{11.7 \pm 1.3}$
Brautigam and Albert [2000]	T89	Empirical field	Diffusion equation	3–6.5	100 to 1000	*Kp*-dependent *dB*	10^{-4} to 10^{2}	L^{10}
Elkington et al. [2003]	Compressed dipole	Analytical field	Test particle	6.6	1870	dE = 0.6 mV/m	1.02	
Brautigam et al. [2005]	Dipole	CRRES E-field	Diffusion equation	3–7	500 and 5000	*Kp*-dependent *dE*	10^{-5} to 10^{1}	$L^{-1.31}$ to $L^{3.77}$
Perry et al. [2006]	Dipole	Analytical field	Test particle	4–6.6	273	dB = 20 nT	10^{-2} to 10^{1}	L^{12}
Fei et al. [2006]	Compressed dipole	Analytical field	Diffusion equation	2–10	1870	dB = 20 nT	10^{-3} to 10^{3}	$L^{8.5}$
This work	LFM	LFM V_x simulations	Test particle	4–10	1800	dB = 1 and 2 nT	10^{-4} to 10^{-0}	$L^{7.5}$ and $L^{10.6}$

[a]Magnetic field model, wave field, calculating method of solving D_{LL}, radial distance in *L*, electron energy in *M*, average wave amplitude at geosynchronous orbit (*dB* or *dE*), derived D_{LL} values and *L*-dependence of D_{LL}.

particle simulation results demonstrate the radial diffusion coefficient is larger for equatorially mirroring electrons. Therefore, following 90 degree pitch angle particle is sufficient to characterize the general behavior of radiation belt particles at most other pitch angles while the transport/heating by the MHD waves is most effective in the equatorial plane. In addition, from a purely practical consideration, the computational requirement is much less when tracing 90 degree pitch angle particles.

[21] Test particles are launched with a fixed first adiabatic invariant, M = 1800 MeV/G, equivalent to ~1 MeV electrons at geosynchronous orbit. The radial distributions of the particles are from 4 to 8 R_E, with an increment of 0.1 R_E. In the azimuthal direction, particles are evenly distributed every one degree. For both V_x = 400 and 600 km/s runs, we follow the guiding center trajectories of ~15000 particles. For radial distance from 4 to 8 R_E, the electron energies are between 0.6 and 2.6 MeV, the electron drift periods are between 6.5 and 18 minutes, and the drift frequencies are between 0.8 and 2.2 mHz. With the same initial starting locations, electrons finish at different radial locations after experiencing different levels of field fluctuations in the two simulations. In the higher solar wind velocity simulation, electrons diffuse outward to greater radial distances and more particles are lost to magnetopause. As a preliminary and expected qualitative conclusion, electrons experience higher radial transport when the wave field is stronger.

[22] To quantify the electron radial transport rate excluding the *Dst* effect, we convert the particle locations to "*L* shell," a quantity used to describe the radial distance of trapped energetic particles. The commonly used L values are the McIlwain L_M [*McIlwain*, 1961] and the generalized L^* [*Roederer*, 1970]. L_M value is defined based on the instantaneous magnetic field configuration of a given field line and is computationally cheap. It is widely used for radiation belt analysis despite the fact that it does not represent the third adiabatic invariant in this region (i.e., it is a local not a global measure), especially during high magnetic activity. On the other hand, L^* depends inversely on Φ, the total magnetic flux enclosed by the drift orbit of an electron [*Roederer*, 1970]:

$$L^* = -\frac{2\pi k_0}{R_E \Phi}, \tag{3}$$

where k_0 is the magnetic moment of Earth's dipole. We calculate the more rigorously correct global L^* values in MHD fields following the methodology of *Roederer* [1970]: (1) follow a particle trajectory in the equatorial plane; (2) trace the field lines which thread the particle's trajectory to Earth's surface; and (3) integrate the magnetic flux over the area defined by the mapped trajectory at Earth's surface. Essentially, until now, computational speed has limited the use of this physically correct approach; we adopt it in our analysis.

[23] After converting the particle's initial and final locations to L^*, base on equation (2), we calculate the D_{LL} values of the ensemble of test particles and bin them according to initial radial distance L_0^*. Figure 5 illustrates the radial diffusion coefficient D_{LL} of the MHD V_x simulations as a function of solar wind velocity. The D_{LL} values of the V_x = 400 and 600 km/s runs are plotted in blue circles and green diamonds, respectively. The linear fits of the D_{LL} values on

a logarithmic scale are also shown. The radial diffusion rates are higher at larger radial distance and during higher solar wind velocity. The slopes of the two sets of D_{LL} values are different just as were the results of the different radial distributions of the E_ϕ wave power in the MHD V_x simulations, as shown earlier in Figure 4. The L shell dependence of the V_x = 400 and 600 km/s simulations are $L^{7.5}$ and $L^{10.6}$, respectively. In section 4, we compare the calculated radial diffusion rates with previous studies and discuss the similarities and differences.

4. Comparison of Radial Diffusion Coefficients

[24] Direct comparison with previous relevant estimates of the diffusion coefficients is somewhat challenging owing to differences in ULF wave power, electron energy, field models, and observations between the studies. A chronological summary of recent radial diffusion studies is provided in Table 1, along with our results. We compare and discuss the similarities and differences between the studies for the use of magnetic field model, wave field, radial distance, particle energy, wave amplitude and derived D_{LL} values.

[25] While most of the D_{LL} studies use a dipole field, a compressed dipole field, or early versions of the Tsyganenko model, our work uses a well developed global MHD code as the field model, which has the advantage of being time-dependent, self-consistent and driven realistically by time-dependent solar wind inputs. Even during a very quiet interval, the magnetospheric configuration is far from a dipole, especially at higher radial distances and during stronger field disturbances. A dipole or a near-dipole thus limits some previous D_{LL} estimates.

[26] Other than *Selesnick et al.* [1997] which uses Polar energetic particle measurements to derive D_{LL} directly, the other recent studies derive or simulate particle radial transport in wave fields, whether theoretical or empirical. *Brautigam and Albert* [2000], *Elkington et al.* [2003], *Brautigam et al.* [2005], and *Fei et al.* [2006] solve the radial diffusion equation with the electron phase space density as a function of prescribed wave fields. The wave field description of *Brautigam and Albert* [2000] is a coarse collection of ground and space measurements as a function of *Kp* at sparse points in the space. *Elkington et al.* [2003] use an analytical field that approximately simulates the characteristics of global Pc5 ULF waves. *Brautigam et al.* [2005] calculate D_{LL}^E based on CRRES electric field measurements as a function of *Kp* and *L*. *Fei et al.* [2006] solve the radial diffusion equation based on an analytical wave field using wave power calculated from the LFM MHD simulations. On the other hand, *Perry et al.* [2006] follow test particles in the analytical wave field with amplitudes based on ground wave measurements. In other words, each study has slight to significant differences in their approach. In our study, we also follow test particles to simulate radial diffusion but the wave fields are realistic MHD model predictions driven by idealized solar wind and IMF conditions.

[27] The radial distance among the studies in Table 1 range from L = 2 to L = 10, although the studies used a mixture of McIlwain L_M and Roederer L*, thereby confounding direct comparisons. The particle energies in these studies range from M = 100 to 6000 MeV/G which should reflect different energy-dependent D_{LL} values. The true energy dependence of the D_{LL} value is not well known due to the complexity of wave-particle interactions and lack of knowledge of the field configuration.

[28] The level of wave fields also varies between the works. Some are statistical studies over a period of time, such as *Selesnick et al.* [1997]. Some wave fields have *Kp* dependence based on magnetic and electric field observations, such as *Brautigam and Albert* [2000] and *Brautigam et al.* [2005]. Analytical field models are used by *Elkington et al.* [2003] and *Perry et al.* [2006], a flexible approach for exploring the particle drift resonances in different wave modes. *Fei et al.* [2006] use an analytical wave field with storm time wave power calculated from the LFM MHD simulations. Finally, our work uses the wave fields calculated from the MHD simulations to study particle radial diffusion during relatively quiet intervals. In sum, the second to last column of Table 1 demonstrates the large deviation between the D_{LL} values, over several orders of magnitude, due to the different observations, assumptions, and techniques used in each study. The L-dependence of radial diffusion coefficients based on magnetic field, D_{LL}^M, are in a range between $L^{7.5}$ and L^{12}.

[29] For the reasons noted above, while a direct comparison between these studies might not be appropriate, because D_{LL} values vary for different assumptions or conditions upon which they are based, we summarize the various diffusion rates in Figure 6 to compare with our results. Most of the D_{LL} values are plotted in lines, except the single-point estimation by *Elkington et al.* [2003], the wave mode study by *Perry et al.* [2006] and the *Kp*-dependent wave field studies by *Brautigam and Albert* [2000] and *Brautigam et al.* [2005]. The single-point estimation is marked by a black circle, and the wave mode and activity studies are plotted in colored outline areas. Compared to previous results, both sets of our D_{LL} values are lower. We believe this is in part because our pressure-driven V_x simulations predict very quiet intervals generally not considered in other studies. The only variation driving the MHD code is solar wind dynamic pressure changes between 1.0 and 2.5 nPa and with a steadily northward IMF B_z of 2 nT. Under these relatively gentle interplanetary driving conditions, the average wave amplitude (dB) at geosynchronous orbit is 1 and 2 nT for the V_x = 400 and 600 km/s runs, which is ten and five times smaller than the *Selesnick et al.* [1997] values at geosynchronous orbit (the field perturbations of *Selesnick et al.* [1997] are estimated from the GOES-8 data during the 3 month interval).

[30] The effect of ULF waves on the radial transport of energetic electrons is a nonlinear process. However, if we assume the amount of radial transport is proportional to the level of field fluctuation, then we can compare the diffusion rates after being scaled by the wave amplitude. For example, while the wave amplitude of *Selesnick et al.* [1997] is 10 and 5 times higher than our V_x = 400 and 600 km/s simulations, we multiply our D_{LL} values 100 and 25 times because D_{LL} is proportional to the square of field fluctuations ($D_{LL} \propto dB^2$) [*Schulz and Lanzerotti*, 1974]. The correlation between D_{LL} and wave amplitude only works for quiet times because the spectral properties and spatial distribution of ULF waves may change during disturbed conditions and the radial diffusion coefficient will not be proportional to dB^2 [*Perry et al.*, 2006]. Figure 7 shows the comparisons between previ-

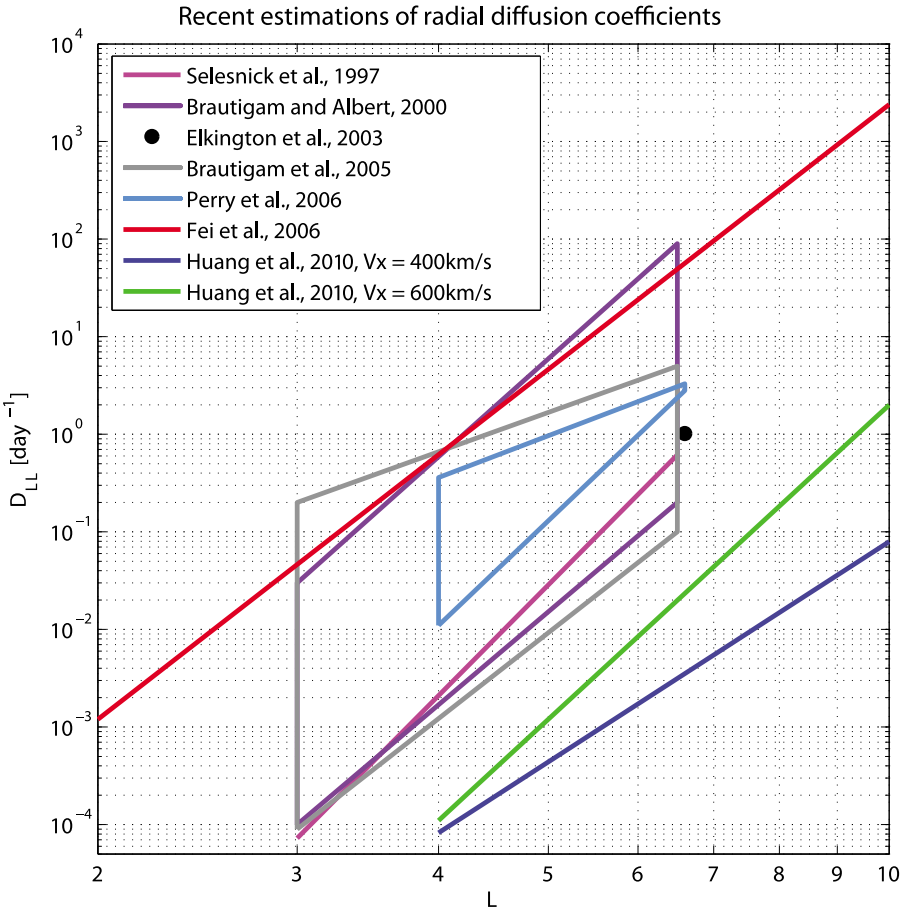

Figure 6. Comparison of radial diffusion coefficients D_{LL} between our simulations results with recent estimations. *Selesnick et al.* [1997], *Fei et al.* [2006] and our results are plotted in colored lines. *Brautigam and Albert* [2000], *Brautigam et al.* [2005], and *Perry et al.* [2006] are in colored outlined areas. *Elkington et al.* [2003] is plotted in single black circle.

ous studies and our scaled D_{LL} values based on normalized wave amplitudes. After the normalization based on wave amplitudes, our D_{LL} results for V_x = 600 km/s are strikingly comparable to *Selesnick et al.* [1997]. Although the average solar wind velocity of the 3 month interval from *Selesnick et al.* [1997] is 400 km/s, there are several high speed stream events during that period which may dominate the wave fields. Consequently, this may explain why their observational results are similar to our scaled D_{LL} values for the V_x = 600 km/s event. As mentioned earlier, the LFM code we used for particle simulation does not include a plasmasphere model which allows ULF wave power to penetrate deeper than it would with a plasmasphere. While *Selesnick et al.* [1997] corresponds to scattering rates inside the plasmasphere, our radial diffusion rates can only be used outside the plasmasphere.

5. Summary

[31] In this paper, we use the pressure-driven MHD simulations as a function of solar wind velocity to study the effects of ULF waves on radiation belt electrons by calculating the rate of radial diffusion. A new technique was developed to generate solar wind data that characterizes the pressure variations of a particular solar wind velocity based on statistical measurements. By driving the MHD code with the synthetic pressure profiles and northward IMF B_z, we generate MHD simulations that represent realistic solar wind V_x conditions and which isolate other drivers. Compared to statistical results of GOES data under similar conditions, these pressure-driven V_x MHD simulations produce qualitatively and quantitatively reasonable ULF wave power. Wave power in both magnetic and electric fields grows stronger for higher solar wind V_x events mainly because of the higher pressure fluctuations that generate compressional waves. The ULF wave amplitude increases at larger radial distance on the dayside at a location closer to the source of the driving disturbance at the magnetopause.

[32] The LFM MHD code not only provides realistic, global, time-dependent and self-consistent fields, but also produces a realistic ULF wave power that an analytical wave field cannot. By following the test particles in the pressure-driven V_x simulations, we determined radial diffusion rates of 90 degree pitch angle electrons at the equatorial plane. When compared with previous studies, our radial diffusion coefficients are smaller, principally because of the much lower ULF wave power of our study relative to other studies. After scaling the D_{LL} values based on the relative wave amplitudes, our results are equivalent to the radial diffusion coefficient calculated from particle mea-

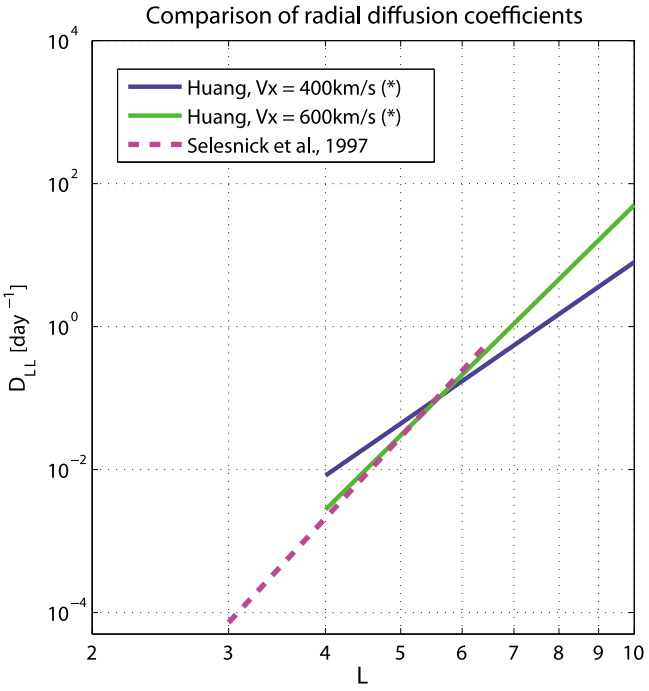

Figure 7. Comparison of radial diffusion coefficients between *Selesnick et al.* [1997] and our scaled D_{LL} values based on the wave amplitude used in the studies.

surements by *Selesnick et al.* [1997]. This technique of estimating radial diffusion rate for controlled solar wind velocity can be extended to isolating other solar wind conditions or geomagnetic activity to quantify the ULF wave effects on radiation belt electrons. Such a method was suggested years ago by *Walt* [1994], but could not be performed until the recent development of global MHD code and our quantitative validation of the LFM code. This accomplishment enabled us to quantify effects of ULF waves on radiation belt electrons and to differentiate this radial diffusive process from other particle acceleration, transport and loss mechanisms.

[33] **Acknowledgments.** We thank W. J. Hughes and J. G. Lyon for helpful discussions and suggestions. We acknowledge the WDC for Geomagnetism, Kyoto University, Japan for the geomagnetic indices, and CDA Web for GOES and Wind data. This material is based upon work supported by Center for Integrated Space Weather Modeling (CISM) funded by the Science and Technology Centers Program of the National Science Foundation under agreement ATM-0120950 and by the NASA Radiation Belt Storm Probes (RBSP) mission funded under JHU/APL subcontract 923497 of prime NASA contract NAS5-01072.

[34] Zuyin Pu thanks the reviewer for his/her assistance in evaluating this paper.

References

Baker, D. N., et al. (1998), A strong CME-related magnetic cloud interaction with the earth's magnetosphere: ISTP observations of rapid relativistic electron acceleration on May 15, 1997, *Geophys. Res. Lett.*, *25*, 2975–2978, doi:10.1029/98GL01134.

Brautigam, D. H., and J. M. Albert (2000), Radial diffusion analysis of outer radiation belt electrons during the October 9, 1990, magnetic storm, *J. Geophys. Res.*, *105*, 291–309, doi:10.1029/1999JA900344.

Brautigam, D. H., G. P. Ginet, J. M. Albert, J. R. Wygant, D. E. Rowland, A. Ling, and J. Bass (2005), CRRES electric field power spectra and radial diffusion coefficients, *J. Geophys. Res.*, *110*, A02214, doi:10.1029/2004JA010612.

Elkington, S. R., M. K. Hudson, and A. A. Chan (1999), Acceleration of relativistic electrons via drift-resonant interaction with toroidal-mode Pc-5 ULF oscillations, *Geophys. Res. Lett.*, *26*, 3273–3276, doi:10.1029/1999GL003659.

Elkington, S. R., M. K. Hudson, and A. A. Chan (2003), Resonant acceleration and diffusion of outer zone electrons in an asymmetric geomagnetic field, *J. Geophys. Res.*, *108*(A3), 1116, doi:10.1029/2001JA009202.

Elkington, S. R., M. Wiltberger, A. A. Chan, and D. N. Baker (2004), Physical models of the geospace radiation environment, *J. Atmos. Sol. Terr. Phys.*, *66*, 1371–1387.

Fälthammar, C.-G. (1965), Effects of time-dependent electric fields on geomagnetically trapped radiation, *J. Geophys. Res.*, *70*(11), 2503–2516.

Fei, Y., A. A. Chan, S. R. Elkington, and M. J. Wiltberger (2006), Radial diffusion and MHD particle simulations of relativistic electron transport by ULF waves in the September 1998 storm, *J. Geophys. Res.*, *111*, A12209, doi:10.1029/2005JA011211.

Friedel, R. H. W., G. D. Reeves, and T. Obara (2002), Relativistic electron dynamics in the inner magnetosphere—A review, *J. Atmos. Sol. Terr. Phys.*, *64*, 265–282, doi:10.1016/S1364-6826(01)00088-8.

Green, J. C., and M. G. Kivelson (2004), Relativistic electrons in the outer radiation belt: Differentiating between acceleration mechanisms, *J. Geophys. Res.*, *109*, A03213, doi:10.1029/2003JA010153.

Horne, R. B., and R. M. Thorne (1998), Potential waves for relativistic electron scattering and stochastic acceleration during magnetic storm, *J. Geophys. Res.*, *25*, 3011–3014, doi:10.1029/98GL01002.

Huang, C.-L., H. E. Spence, J. G. Lyon, F. R. Toffoletto, H. J. Singer, and S. Sazykin (2006), Storm-time configuration of the inner magnetosphere: Lyon-Fedder-Mobarry MHD code, Tsyganenko model, and GOES observations, *J. Geophys. Res.*, *111*, A11S16, doi:10.1029/2006JA011626.

Huang, C.-L., H. E. Spence, H. J. Singer, and W. J. Hughes (2010), Modeling radiation belt radial diffusion in ULF wave fields: 1. Quantifying ULF wave power at geosynchronous orbit in observations and in global MHD model, *J. Geophys. Res.*, *115*, A06215, doi:10.1029/2009JA014917.

Hudson, M. K., S. R. Elkington, J. G. Lyon, C. C. Goodrich, and T. J. Rosenberg (1999), Simulation of radiation belt dynamics driven by solar wind variations, in *Sun-Earth Plasma Connections*, *Geophys. Monogr. Ser.*, vol. 109, edited by J. L. Burch, R. L. Carovillano, and S. K. Antiochos, p. 171–182, AGU, Washington, D. C.

Hudson, M. K., S. R. Elkington, J. G. Lyon, and C. C. Goodrich (2000), Increase in the relativistic electron flux in the inner magnetosphere: ULF wave mode structure, *Adv. Space Res.*, *25*, 2327–2337.

Hudson, M. K., B. T. Kress, H.-R. Mueller, J. A. Zastrow, and J. B. Blake (2008), Relationship of the Van Allen radiation belts to solar wind drivers, *J. Atmos. Sol. Terr. Phys.*, *70*(5), 708–729.

Kellogg, P. G. (1959), Van Allen radiation of solar origin, *Nature*, *183*, 1295–1297, doi:10.1038/1831295a0.

Kepko, L., H. E. Spence, and H. J. Singer (2002), ULF waves in the solar wind as direct drivers of magnetospheric pulsations, *Geophys. Res. Lett.*, *29*(8), 1197, doi:10.1029/2001GL014405.

Lanzerotti, L. J., C. G. MacLennan, and M. Schulz (1970), Radial diffusion of outer-zone electrons: An empirical approach to third-invariant violation, *J. Geophys. Res.*, *75*, 5351–5371.

Lyon, J. G., J. A. Fedder, and C. M. Mobarry (2004), The Lyon-Fedder-Mobarry (LFM) global MHD magnetospheric simulation code, *J. Atmos. Sol. Terr. Phys.*, *66*, 1333–1350.

McIlwain, C. E. (1961), Coordinates for mapping the distribution of magnetically trapped particles, *J. Geophys. Res.*, *66*, 3681–3691.

Nakada, M. P., and G. D. Mead (1965), Diffusion of protons in the outer radiation belt, *J. Geophys. Res.*, *70*(19), 4777–4791.

Parker, E. N. (1960), Geomagnetic fluctuations and the form of the outer zone of the Van Allen radiation belt, *J. Geophys. Res.*, *65*(10), 3117–3130.

Paulikas, G. A., and J. B. Blake (1979), Effects of the solar wind on magnetospheric dynamics: Energetic electrons at the synchronous orbit, in *Quantitative Modeling of Magnetospheric Processes*, *Geophys. Monogr. Ser.*, vol. 21, edited by W. P. Olsen, pp. 180–202, AGU, Washington, D. C.

Perry, K. L., M. K. Hudson, and S. R. Elkington (2005), Incorporating spectral characteristics of Pc5 waves into three-dimensional radiation belt modeling and the diffusion of relativistic electrons, *J. Geophys. Res.*, *110*, A03215, doi:10.1029/2004JA010760.

Perry, K. L., M. K. Hudson, and S. R. Elkington (2006), Correction to "Incorporating spectral characteristics of Pc5 waves into three-dimensional radiation belt modeling and the diffusion of relativistic electrons", *J. Geophys. Res.*, *111*, A11228, doi:10.1029/2006JA012040.

Roederer, J. G. (1970), *Dynamics of Geomagnetically Trapped Radiation*, Springer, New York.

Rostoker, G., S. Skone, and D. N. Baker (1998), On the origin of relativistic electrons in the magnetosphere associated with some geomagnetic storms, *Geophys. Res. Lett.*, *25*, 3701–3704, doi:10.1029/98GL02801.

Schulz, M., and L. J. Lanzerotti (1974), in *Particle Diffusion in the Radiation Belt*, Springer, New York.

Selesnick, R. S., J. B. Blake, W. A. Kolasinski, and T. A. Fritz (1997), A quiescent state of 3 to 8 MeV radiation belt electrons, *Geophys. Res. Lett.*, *24*, 1343–1346, doi:10.1029/97GL51407.

Shprits, Y. Y., S. R. Elkington, N. P. Meredith, and D. A. Subbotin (2008a), Review of modeling of losses and sources of relativistic electrons in the outer radiation belt I: Radial transport, *J. Atmos. Sol. Terr. Phys.*, *70*, 1679–1693, doi:10.1016/j.jastp.2008.06.008.

Shprits, Y. Y., D. A. Subbotin, N. P. Meredith, and S. R. Elkington (2008b), Review of modeling of losses and sources of relativistic electrons in the outer radiation belt II: Local acceleration and loss, *J. Atmos. Sol. Terr. Phys.*, *70*, 1694–1713, doi:10.1016/j.jastp.2008.06.014.

Summers, D., R. M. Thorne, and F. Xiao (1998), Relativistic theory of wave-particle resonant diffusion with application to electron acceleration in the magnetosphere, *J. Geophys. Res.*, *103*, 20,487–20,500, doi:10.1029/98JA01740.

Walt, M. (1994), *Introduction to Geomagnetically Trapped Radiation*, Cambridge Univ. Press, New York.

S. R. Elkington, Laboratory for Atmospheric and Space Physics, University of Colorado, 1234 Innovation Dr., Boulder, CO 80303, USA.

C.-L. Huang and H. E. Spence, Center for Space Physics, Boston University, 725 Commonwealth Ave., Boston, MA 02215, USA. (hcl@bu.edu)

M. K. Hudson, Department of Physics and Astronomy, Dartmouth College, 6127 Wilder Laboratory, Hanover, NH 03755, USA.